J. Fluid Mech. (2010), *vol.* 663, *pp.* 209–232. © Cambridge University Press 2010
doi:10.1017/S0022112010003472

Dynamics of gas bubbles in time-variant temperature fields

I. R. WEBB[1], M. ARORA[1], R. A. ROY[2], S. J. PAYNE[1] AND C.-C. COUSSIOS[1]†

[1]Institute of Biomedical Engineering, Department of Engineering Science, University of Oxford, Oxford OX1 3PJ, UK

[2]Department of Aerospace and Mechanical Engineering, Boston University, Boston, MA 02215, USA

(Received 18 March 2010; revised 23 June 2010; accepted 25 June 2010; first published online 17 September 2010)

The effect of time-variant temperature on the dynamics of a single gas bubble in a liquid is investigated. With changes in temperature, several physical parameters controlling bubble behaviour change including surface tension, diffusivity, vapour pressure and gas solubility. A single-bubble model is formulated and a numerical simulation implemented to model the radius–time profile of a bubble, across a range of initial bubble sizes and rates of heating, taking into account the aforementioned parameter temperature dependences. The model is validated experimentally in a xanthan gum gel phantom, tracking the evolution of the bubbles using digital photography and an image analysis sizing algorithm. It is shown that the natural tendency for a bubble to dissolve can be reversed by an increase in temperature, but only above a certain radius-dependent threshold rate of heating.

Key words: bubble dynamics

1. Introduction

The dynamics of gas bubbles in liquids and viscoelastic materials have been studied for almost a century (Rayleigh 1917). However, the majority of these studies neglect the effect of changing temperature on the key parameters – surface tension, diffusivity, vapour pressure and gas solubility – that control the growth or dissolution of a bubble, instead assuming constant, temperature-independent values.

Several emerging applications now require a deeper understanding of the effects of heating and cooling on bubble dynamics. Those include: cavitation mitigation in spallation neutron sources (Riemer *et al.* 2005); improving the performance of chemical processes in bubble column reactors and multiphase slurries (Schafer, Merten & Eigenberger 2002); and the development of minimally invasive and non-invasive medical procedures that use or involve acoustic cavitation to modify tissue or deliver drugs (Coussios & Roy 2008). In the context of biomedical applications, this study is of particular relevance to the use of high intensity focused ultrasound for the thermal ablation of deep-seated tumours and other tissues. During the course of such treatments, bubbles can either be spontaneously nucleated due to the high rarefactional pressures attained at the ultrasound focus, or larger vapour cavities can form due to tissue boiling. Subsequent cavitation effects can be utilized to improve treatment

† Email address for correspondence: constantin.coussios@eng.ox.ac.uk

https://doi.org/10.1017/S0022112010003472 Published online by Cambridge University Press

efficacy as well as showing potential for use in real-time treatment monitoring, whilst suppression of cavitation is also sometimes desirable for improved treatment safety (Rabkin, Zderic & Vaezy 2005). Even though the effects of acoustic excitation are not explicitly investigated in this study, the heating profiles and range of temperature rises investigated have been chosen so as to be relevant to ultrasound-induced tissue heating. In particular, this study is relevant to understanding and modelling bubble growth or dissolution as a result of heating or cooling. Changes to the size ranges present within a particular bubble population can directly impact on the type of cavitation activity that will be observed under acoustic excitation (Church 2005).

Epstein & Plesset (1950) were among the first to study the behaviour of bubbles in a liquid–gas solution at a constant (room) temperature. The analysis included a number of important simplifying assumptions to allow a basic analytical solution of the diffusion equation alone, arriving at the radius–time evolution of the bubbles. Studies since, on the growth and dissolution of both gas and vapour bubbles, have used the diffusion equation alongside an equation of motion and have employed solution methods ranging from similarity solutions (see Scriven 1959; Cable & Frade 1987) to perturbation and numerical solutions (see Barlow & Langlois 1962). A numerical solution is required if the bubble evolution is to be accurately modelled, as the highly coupled nature of the diffusion equation and the bubble equation of motion means no analytical solution exists for the generalized problem (see Arefmanesh, Advani & Michaelides 1992).

Scriven (1959) and Miyatake, Tanaka & Lior (1994) are amongst those who have investigated bubble behaviour at elevated temperatures, both considering vapour-bubble growth in superheated solutions. Their analyses focused on heat and mass transfer controlled growth at a constant temperature, rather than the bubble dynamics due to an imposed temperature profile, and hence it was not necessary to consider changing values of temperature-dependent parameters. In a similar study of water vapour bubbles in perlite at high temperatures ($\sim$1000 °C), it was necessary for Zahringer, Martin & Petit (2001) to consider temperature-dependent parameters, as energy lost to the evaporation of the water resulted in a temperature drop during the course of the simulation. However, it is clear that this temperature change is not an imposed variation as is the case with ultrasonic heating.

Imposed temperature fields have been considered by Robinson & Judd (2001), who investigated the growth of hemispherical vapour bubbles in a spatially distributed temperature field; however, it was necessary to artificially perturb the bubbles to initiate growth. It is not noted whether the temperature field was temporally as well as spatially variant. Divinis *et al.* (2005) considered the problem of a vapour bubble growing around an embedded miniature heater for a limited range of conditions that result in self-similar growth. Some variation of temperature-dependent parameters was explored, but these variations were approximated to fit with the self-similar solution rather than follow the exact dependence. As this study considered vapour bubbles, bubble sizes and growth rates were significantly greater than those expected in a gas-diffusion controlled process. In the study of Fan, Mitchell & Blanshard (1999), dough expansion – by the way of bubble growth – was considered during constant-rate heating, with the temperature dependences of Henry's constant and vapour pressure incorporated into the model. Throughout the rising process, the gas-concentration profile in the surrounding medium remains spatially uniform and the time-dynamics of the diffusion process seem to have been neglected.

https://doi.org/10.1017/S0022112010003472 Published online by Cambridge University Press

In summary, there has been significant study of bubble dynamics in liquid–gas solution, but the generalized problem considering the dynamics of gas-bubble growth or dissolution resulting from an imposed change in temperature has not been fully addressed in these studies. The solution to the generalized problem is affected by several factors that have opposing influences. With an increase in temperature, gas within a bubble will expand and vapour pressure also increases, which would ordinarily cause a bubble to expand. Additionally, the solubility of gas in liquids decreases as temperature rises, making the process of gas diffusion into a bubble more favourable at higher temperatures. However, the natural tendency for a bubble in solution is to dissolve away, as the pressure within the bubble is higher due to surface tension effects. The ultimate fate of a bubble – whether it grows or dissolves away – will be dependent on the relative contributions of these effects.

In this paper, the traditional model of a gas bubble in liquid is extended so as to simulate the response of a bubble to an arbitrary heating input. The model presented incorporates the temperature dependence of four parameters relevant to diffusion-controlled bubble dynamics – surface tension, solubility (in the form of Henry's constant), vapour pressure and diffusion coefficient. The complexity of the model, even before the addition of the temperature-dependent terms, necessitates the use of a finite-difference-based numerical solver to accurately predict the evolution of the bubble over time.

To validate the predictions of the numerical solver, an experimental set-up has been devised to allow the optical tracking and sizing of bubbles entrapped within a xanthan gum gel phantom. By inputting the temperature profiles obtained during the experiments into the numerical solver, direct comparison between theory and experiment is possible, and subsequent refinements to the model are suggested on the basis of the differences observed.

2. Single-bubble model

A single-bubble model is formulated, in spherical coordinates, to determine the response of a bubble to arbitrary heating inputs. The following assumptions are made in this analysis to allow construction of the model.

(i) The bubble remains perfectly spherical at all times, allowing the problem to be considered in a single dimension.

(ii) Temperature across the bubble, and its surrounding shell of liquid, is assumed to be spatially uniform. The transport parameters are, therefore, not spatially dependent, and can be determined by temperature alone.

(iii) Bubble growth and dissolution is driven by the mass diffusion of the dissolved gas, a slow process taking place over tens or hundreds of seconds, making the contributions from inertial and convection effects negligible.

(iv) The water vapour pressure can be determined from temperature alone, as thermodynamic equilibrium is maintained by rapid vapour transfer at the bubble wall given the distance and time scales in question.

The model can broadly be divided into three parts: an equation of motion to describe changes in bubble radius, mass diffusion of gas through the bubble wall and the temperature dependence of the relevant physical parameters. These aspects of the model are described in the following sections.

https://doi.org/10.1017/S0022112010003472 Published online by Cambridge University Press

2.1. *Equation of motion*

The Rayleigh–Plesset equation is commonly used to model the change in bubble radius R with time t due to an incident pressure field

$$R\ddot{R} + \frac{3}{2}\dot{R}^2 = \frac{1}{\rho_L}\left[p_g + p_v - p_\infty - \frac{2\sigma}{R} - \frac{4\eta\dot{R}}{R} - p_{ac}\right], \tag{2.1}$$

where p_g and p_v are the gas and vapour pressures within the bubble, respectively, p_∞ is the ambient liquid pressure, σ is the surface tension coefficient, ρ_L is the liquid density, η is the viscosity, p_{ac} is an acoustic forcing term and the dot notation represents differentiation with respect to time.

In this study, the effect of acoustics is neglected, meaning that the bubble radius is controlled by diffusion effects. Changes in the bubble size occur slowly and hence the magnitudes of the bubble-wall velocity $\dot{R}$ and acceleration $\ddot{R}$ are small. The contribution of the inertial terms, and that of the viscous stress $4\eta\dot{R}/R$, can therefore be neglected as they are small relative to the magnitudes of the pressure terms. The result is that a static pressure balance is sufficient to define the variation of the bubble radius over time:

$$p_g + p_v = p_\infty + \frac{2\sigma}{R}. \tag{2.2}$$

As there exist only two unknown variables – internal gas pressure and bubble radius – a single equation of state is necessary to close this part of the problem. Due to the importance of mass diffusion in this study, the ideal gas equation is chosen and written in terms of the mass of gas within the bubble m. This allows the formation of an equation relating the gas pressure within the bubble to a time-variant temperature $T(t)$ and the initial state of the bubble, here represented by the '0' subscript:

$$p_g = p_{g0}\frac{m}{m_0}\frac{R_0^3}{R^3}\frac{T(t)}{T_0}. \tag{2.3}$$

Substituting (2.3) into (2.2) and rearranging gives a time-dependent cubic equation to solve for the bubble radius R

$$(p_\infty - p_v)R^3 + 2\sigma R^2 - p_{g0}R_0^3\frac{m}{m_0}\frac{T(t)}{T_0} = 0, \tag{2.4}$$

which can be non-dimensionalized with respect to length, pressure and temperature

$$\left(1 - \frac{p_v}{p_\infty}\right)a^3 + \gamma a^2 - \frac{p_{g0}}{p_\infty}\mu\theta = 0, \tag{2.5}$$

where a, μ and θ are the non-dimensional bubble radius, mass and temperature, respectively, with respect to the initial states and $\gamma = 2\sigma/p_\infty R_0$ is the non-dimensional surface tension.

2.2. *Mass diffusion*

The Laplace pressure, caused by surface tension at the liquid–gas interface, gives rise to a pressure gradient across the bubble wall. This gradient drives a mass diffusion process, resulting in bubble growth or dissolution dependent on the direction of the gradient. Ordinarily, gas bubbles in liquid will dissolve away as the gas pressure within the bubble is higher than the ambient pressure within the liquid, leading to gas diffusing out of the bubble. The rate of mass diffusion $\dot{m}$ is dependent on the diffusion coefficient D, the surface area of the bubble and the concentration gradient

https://doi.org/10.1017/S0022112010003472 Published online by Cambridge University Press

of the gas $\partial c/\partial r$ within the bulk liquid at the bubble wall:

$$\dot{m} = 4\pi R^2 D \left.\frac{\partial c}{\partial r}\right|_{r=R}. \tag{2.6}$$

To calculate the concentration gradient, it is first necessary to know the form of the gas concentration profile $c(r, t)$ in the surrounding liquid. The concentration profile is found by solving the mass diffusion equation in spherical coordinates:

$$\frac{\partial c}{\partial t} + \boldsymbol{v}\cdot\nabla c = D\nabla^2 c = \frac{D}{r^2}\left[\frac{\partial}{\partial r}\left(r^2\frac{\partial c}{\partial r}\right)\right], \tag{2.7}$$

where $\boldsymbol{v}$ is the velocity field of the liquid. Given the assumption of purely radial motion, and taking the liquid as incompressible, the velocity field consists only of a radial component equal to $R^2\dot{R}/r^2$. Using R_0, the equilibrium bubble radius, as a length scale and ω_0, an arbitrary angular frequency, as a time scale, (2.7) is written in non-dimensional form as

$$\frac{\partial c}{\partial \tau} + \frac{a^2\dot{a}}{\zeta^2}\frac{\partial c}{\partial \zeta} = \frac{1}{Pe}\frac{1}{\zeta^2}\frac{\partial}{\partial \zeta}\left(\zeta^2\frac{\partial c}{\partial \zeta}\right), \tag{2.8}$$

where τ is dimensionless time, ζ is the dimensionless radial coordinate and $Pe = R_0^2\omega_0/D$ is the Péclet number.

In an Eulerian view of the fluid, the liquid does not remain static as the bubble changes in size. Following the method of Fyrillas & Szeri (1994) amongst others, a transformation into Lagrangian coordinates is performed, hence tracking particles within the liquid volume with time and therefore ensuring a spatially accurate concentration profile. The Lagrangian coordinate ψ is a measure of volume rather than position, and is defined as

$$\psi = \tfrac{1}{3}(\zeta^3 - a^3), \tag{2.9}$$

so as to fix the bubble wall at a set position ($\psi = 0$). This allows boundary conditions (BC) to be applied at a fixed point rather than on a moving boundary. An added advantage sees the convective term absorbed into the temporal derivative, simplifying solution of the equation. Rewriting the diffusion equation (2.7) and mass flux (2.6) in Lagrangian coordinates gives

$$\frac{\partial c'}{\partial \tau} = \frac{1}{Pe}\frac{\partial}{\partial \psi}\left[(3\psi + a^3)^{4/3}\frac{\partial c'}{\partial \psi}\right] \tag{2.10}$$

and

$$\frac{\mathrm{d}\mu}{\mathrm{d}\tau} = \frac{3a^4}{Pe}\left.\frac{\partial c'}{\partial \psi}\right|_{\psi=0}, \tag{2.11}$$

where the concentration c' has been redefined relative to the initial saturation concentration c_∞, that is $c' = c - c_\infty$.

To solve the diffusion problem, it is assumed that diffusion takes place in a region around the bubble of fixed volume. The initial width of this region is comparable to the diffusion length $L_D \propto \sqrt{Dt_D}$, where t_D is the time over which diffusion is taking place. BC are calculated using Henry's Law, which relates dissolved gas concentrations to gas pressure: at the bubble wall, $c'_w = Hp_g - c_\infty$, whereas on the outer edge of the diffusion layer the gas concentration is assumed to be equal to the initial saturation concentration, i.e. $c'_\infty = 0$. A function to describe the initial gas concentration profile

https://doi.org/10.1017/S0022112010003472 Published online by Cambridge University Press

within the diffusion volume is also required; this is assumed to be the steady-state profile obtained from solving (2.10) with $\partial c'/\partial\tau = 0$ and negligible contribution from the convective term:

$$c'_0 = \frac{c'_{w0}}{(3\psi+1)^{1/3}}. \tag{2.12}$$

A combination of (2.5), (2.10) and (2.11), along with these BC, gives sufficient information to solve the standard problem of a bubble growing or dissolving in a liquid at a constant temperature.

2.3. *Parameter temperature dependence*

The third section of the model considers the temperature dependence of the physical properties that govern bubble dynamics. Increased temperatures result in decreased gas solubility within the bulk liquid, i.e. Henry's constant H is reduced, and lower surface tension σ at the water–air interface. However, both vapour pressure p_v and diffusivity D increase with temperature. The following formulae for the parameter temperature variation in water have been determined empirically from experimental data, and are presented here for the temperature range 20–60 °C (293–333 K). In all cases, the units of the temperature T are Kelvin (K).

The International Association for the Properties of Water and Steam (see IAPWS 1994) gives the following interpolation formula for the variation of the surface tension (units $\mathrm{N\,m^{-1}}$) with temperature:

$$\sigma = 0.2358\theta_c^{1.256}(1-0.625\theta_c), \quad \text{where} \quad \theta_c = 1-\frac{T}{647.1}. \tag{2.13}$$

The variation of vapour pressure with temperature is highly nonlinear, and tabulated values at various temperatures are commonly available as published steam tables. Filimonov (1991) devised an equation to allow computer calculation of these quantities

$$p_v = p_{ref}\exp\left[\left(\frac{T}{T_{ref}}-1\right)\left(22.486\frac{T_{ref}}{T}+0.3182\frac{T}{T_{ref}}-2.9558\right)\right], \tag{2.14}$$

where p_{ref} and T_{ref} are 610 Pa and 273 K, respectively, being the pressure and temperature evaluated at the triple point. This equation is correct to 0.1 % in the temperature range that is considered in this study.

The experimental data of Rettich, Battino & Wilhelm (2000) have been used in this study to form a new simplified empirical relationship for the variation of the oxygen-in-water Henry's constant (units $\mathrm{kg\,m^{-3}\,Pa^{-1}}$) with temperature, accurate to within 1 % over the relevant temperature range ($R^2 = 0.9995$)

$$\frac{1}{H(T)} = 10^7\left(1.387-\frac{339.47}{T}\right), \tag{2.15}$$

and a similar procedure has been carried out using the experimentally determined diffusion coefficients of Han & Bartels (1996), giving the following empirical relationship for the temperature-dependent oxygen-in-water diffusion coefficient (units $\mathrm{m^2\,s^{-1}}$), accurate to within 3 % ($R^2 = 0.993$):

$$D(T) = 10^{-9}\left(19.81-\frac{5305}{T}\right). \tag{2.16}$$

In comparison to the Arrhenius-type fits obtained by the original authors, the newly determined formulae offer simplicity whilst giving sufficient accuracy in their predictions.

https://doi.org/10.1017/S0022112010003472 Published online by Cambridge University Press

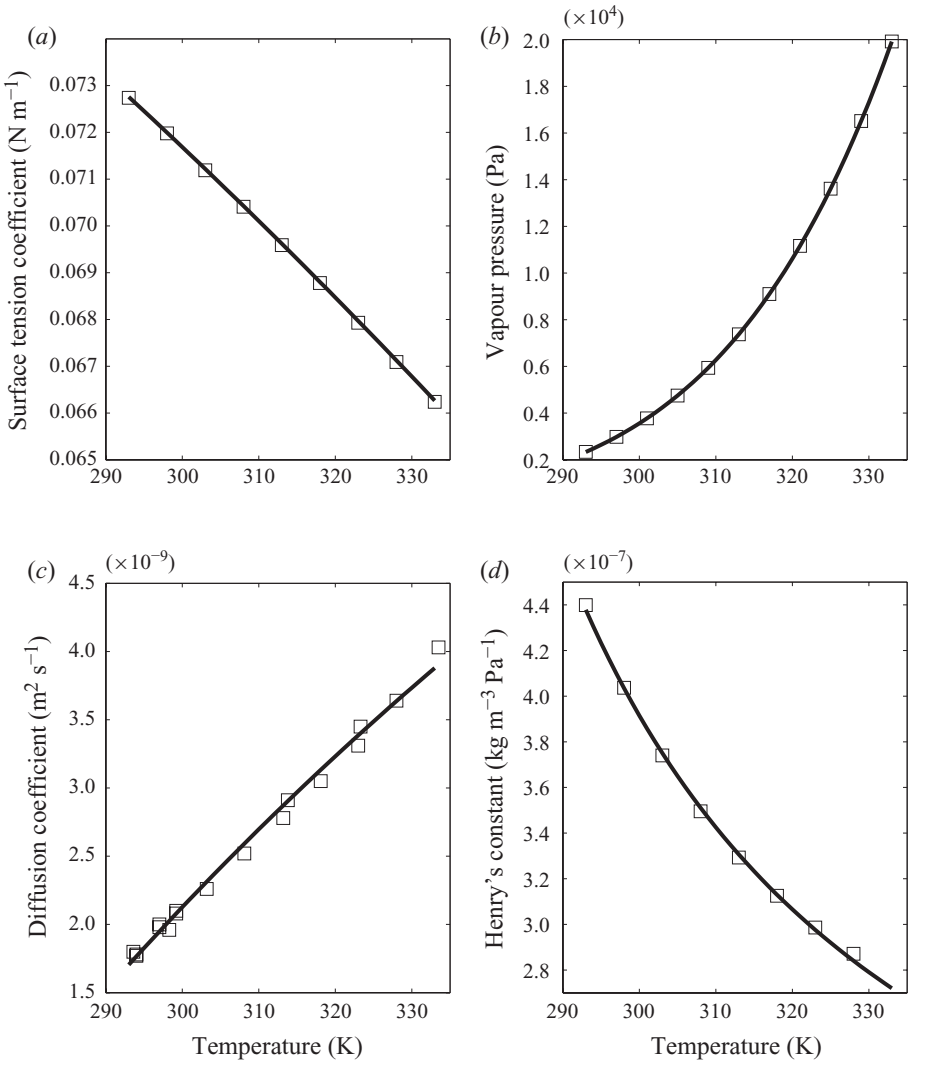


FIGURE 1. Variation in parameter values with temperature in the range 293–333 K for (*a*) surface tension, (*b*) vapour pressure, (*c*) diffusion coefficient and (*d*) Henry's constant. Solid lines represent the empirical relationships of (2.13)–(2.16); the experimental data points (squares) used in forming the empirical relationships are shown for comparison.

The significance of the parameter temperature dependence is shown in figure 1; increasing temperature from 293 to 333 K more than doubles the diffusion coefficient D, increases the vapour pressure p_v by a factor of over 8, decreases the surface tension coefficient σ by 10 % and reduces Henry's constant H by over a factor of 1.5.

3. Numerical solution

As noted in § 1, numerical solutions are necessary for all but the simplest problems in bubble dynamics. The highly coupled nature of the equations of motion and mass diffusion defining this problem necessitates the use of a numerical solver, the algorithm of which is described in figure 2.

https://doi.org/10.1017/S0022112010003472 Published online by Cambridge University Press

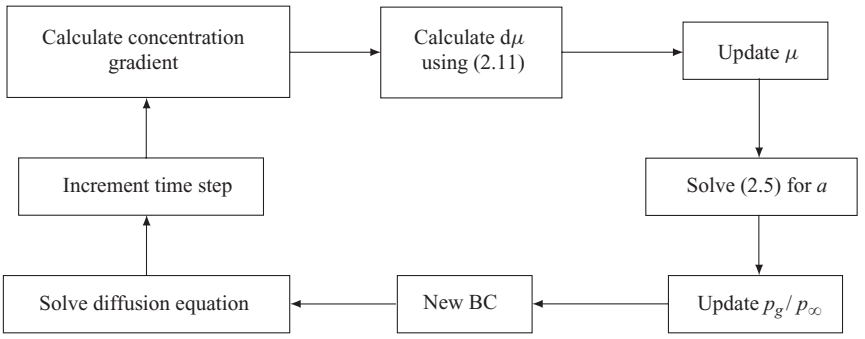


FIGURE 2. Flowchart describing numerical simulation algorithm for each time step.

Inputting the initial conditions into the algorithm at the top left of the flowchart of figure 2 allows calculation of the concentration gradient and subsequent computation of the change in bubble mass. The new bubble radius and gas pressure are then found, the updated BC calculated using Henry's Law, and the diffusion equation solved for the new concentration profile. This process is repeated at each time step, calculating the new values of the temperature-dependent variables, to output the bubble radius–time profiles.

The algorithm will only produce accurate radius–time profiles should the changing mass within the bubble, and hence the mass flux, be calculated accurately. As the calculation of mass flux is reliant on the value of the concentration gradient at the bubble wall, there must be sufficient numerical accuracy in this region of the spatial grid. This is particularly important as the most rapid spatial changes in the concentration profile occur in the region closest to the bubble wall. However, a uniform spatial grid in the Lagrangian coordinate, ψ, results in a rarefaction of the grid points at the bubble wall when viewed in the real-world radial coordinate r. The necessary accuracy required in the solution can be achieved by using a second coordinate transformation that re-concentrates grid points in the region of interest, whilst also maintaining a fixed boundary at the bubble wall. The Lagrangian coordinate ψ is mapped onto the new spatial coordinate y such that $y=0$ at $\psi=0$ and $y=1$ at $\psi=\psi_{max}$, and ensuring $\mathrm{d}y/\mathrm{d}\psi \neq \infty$ at $\psi=0$

$$y = \ln\big(\alpha(\psi+1)^{1/n} + (1-\alpha)\big), \tag{3.1}$$

where

$$\alpha = \frac{\mathrm{e}-1}{(\psi_{max}+1)^{1/n}-1}, \tag{3.2}$$

with n an integer chosen to obtain adequate spatial accuracy in the solution.

The diffusion equations are rewritten in terms of the new spatial coordinate y and solved using the Crank–Nicolson method across a spatial grid spanning the diffusion volume. The spatial derivatives are estimated by an average of the difference approximations at times τ and $\tau+\Delta\tau$, rather than solely at the previous time step; this adds stability to the computation and gives second-order accuracy in both time and space. The set of simultaneous difference equations obtained for the gas concentration c'_{k+1} at each spatial grid-point are written as a tridiagonal matrix, which is inverted to obtain the new spatial concentration profile. From the diffusion equation solution a third-order forward-approximation is used to calculate the concentration gradient

https://doi.org/10.1017/S0022112010003472 Published online by Cambridge University Press

Parameter and units	Value in water	Value range for xanthan gum	Scaling factors
σ (N m^{-1})	0.0721	0.050–0.060	0.69–0.83
H (kg m^{-3} Pa^{-1})	4.10×10^{-7}	$4.05–4.7 \times 10^{-7}$	0.985–1.15
D (m^2 s^{-1})	1.95×10^{-9}	$3.1–4.8 \times 10^{-10}$	0.16–0.245

TABLE 1. Numerical simulation parameter values; all values given at 297 K.

at the bubble wall

$$\left.\frac{\partial c'}{\partial y}\right|_{y=0} = \frac{c'_4 + 9c'_2 - 4.5c'_3 - 5.5c'_1}{3\mathrm{d}y}, \tag{3.3}$$

the solver then continuing around the path detailed in figure 2 for each time step in the period of calculation. Given the parameter values, and the forms of the parameter temperature dependences, the response of a bubble to any variation in temperature can be predicted in any liquid.

4. Model predictions and sensitivity analysis

The single-bubble model and numerical solver formulated in §§ 2 and 3 can be used to predict the response of a bubble to arbitrary temperature variations in both water and xanthan gum. Xanthan gum is a polysaccharide which, on dissolution in water, forms a viscous transparent gel suitable for optical validation of the model predictions. The numerical simulations were based on the response of an oxygen bubble, rather than an air bubble. This was due to the greater availability of parameter data for oxygen in both water and xanthan gum, and overcame the difficulties of accounting for the temperature dependences of more than one gas in solution.

The values of the xanthan gum parameters as determined by Teresaka & Shibata (2003) (table 1) show that the properties of the gel differ, in some cases significantly, from those of water. However, due to the high water content of the xanthan gel, it is assumed that the form of the parameter temperature dependences are identical to those in water. To take account of the differing base values, the temperature dependences of xanthan gum are defined in (2.13)–(2.16) multiplied by an appropriate scaling factor, the values of which are listed in table 1, except for that of vapour pressure (2.14) which is assumed to be identical in both water and xanthan gum. Without further experimental measurements, this is the best approximation available for use in the model. On the numerical grid, a temporal step of 0.01 in τ and a spatial step of 0.01 in the transformed (y) coordinate system was used in the calculations, along with the value for the gas constant for oxygen $R_g = 259.83\,\mathrm{J\,kg^{-1}\,K^{-1}}$, the diffusion layer width $L = 10\,\mathrm{mm}$ and $n = 20$ in the coordinate transformation. The value of ω_0 was chosen such that the non-dimensional time scale τ is equivalent to the dimensional time t.

An arbitrary heating profile (figure 3) is used in the following sections, only for illustrative purposes, to explore the effect and significance of the key parameters on the nature of the bubble response. The profile is obtained from a basic numerical solution of the heat equation in three-dimensional Cartesian coordinates at a point located at a distance from an axisymmetric source.

https://doi.org/10.1017/S0022112010003472 Published online by Cambridge University Press

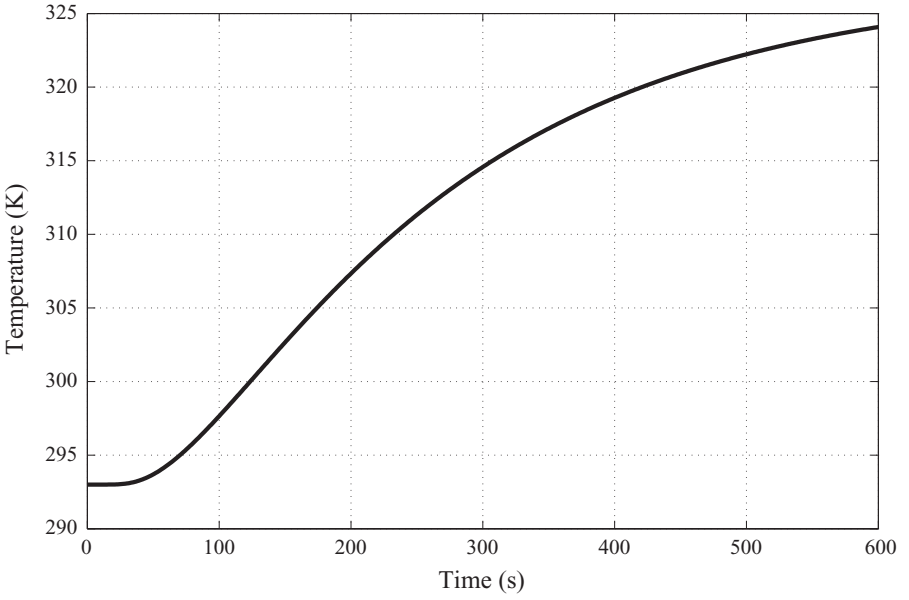


FIGURE 3. Arbitrary heating profile used in numerical simulations.

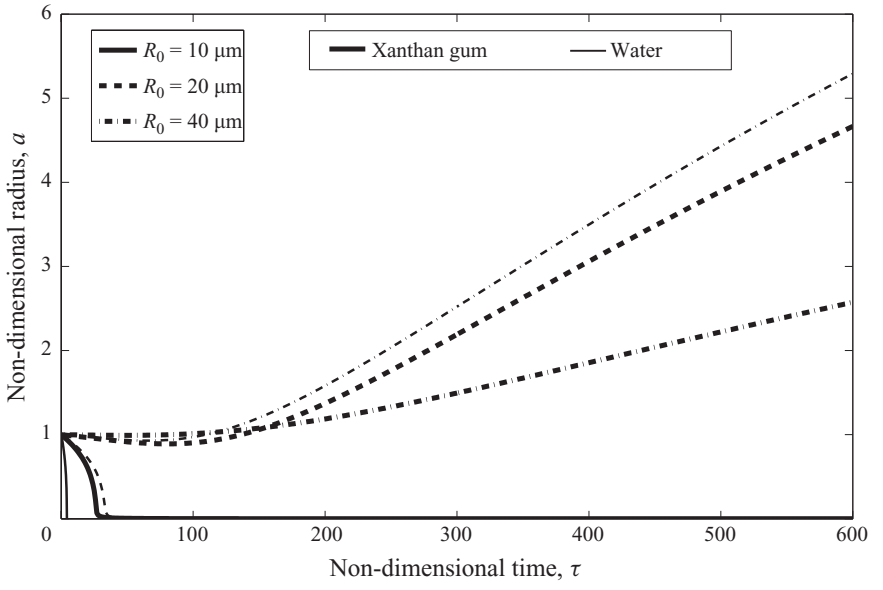


FIGURE 4. Effect of bubble radius on the behaviour of bubbles in response to the heating profile of figure 3. Thicker lines show bubbles in xanthan gum, and thinner lines bubbles in water, at three different initial bubble radii: 10 μm (solid), 20 μm (dashed) and 40 μm (dot-dash).

4.1. *Effect of bubble radius*

Three distinct regimes of behaviour can be seen in the non-dimensional radius–time (a–τ) curves in xanthan gum, dependent on the values of the initial bubble radius R_0. The different types of behaviour are described below and shown in figure 4.

https://doi.org/10.1017/S0022112010003472 Published online by Cambridge University Press

(i) Smaller bubbles show an immediate decrease in bubble size and ultimately bubble dissolution (solid black line).

(ii) Larger bubbles start to expand on heating, and growth continues by diffusion of gas into the bubble once the temperature reaches its upper value (dash-dotted black line). This behaviour is more evident the larger the bubble, as the increase in gas pressure due to surface tension is lower and hence the initial concentration gradient is shallower.

(iii) The third behaviour witnesses intermediate sized bubbles initially shrink as gas diffuses out through the bubble wall. As the temperature increases, the value of Henry's constant decreases; over time the bulk liquid becomes supersaturated and the bubble will begin to grow (dashed black line).

From these observations, it seems that there will be a 'threshold' bubble size for a particular heating profile, above which the bubble will grow. The threshold will depend on the shape and absolute values of the heating profile. It would be expected that the bubble size threshold would decrease as the heating input rate increases, as the gas concentration profile within the liquid changes more rapidly.

Figure 4 also shows that the response of the bubbles to the heating input is highly dependent on the surrounding medium. Bubbles in water, which has a higher diffusion coefficient than xanthan gum, will dissolve away faster, resulting in a greater radius threshold for a specific heating profile. The figure indicates that a bubble in water with a certain initial radius will behave in a similar manner to a bubble in xanthan gum of approximately half that radius.

4.2. *Effect of Henry's constant, diffusion coefficient and surface tension*

The importance of the surrounding medium, and hence the values of the physical parameters governing the bubble behaviour, has been noted in the § 3. The parameters for xanthan gum in table 1 demonstrate some variability in the measured values of surface tension, Henry's constant and diffusion coefficient. To understand the effect of these variations on bubble behaviour, the response of a bubble in xanthan gum with initial radius of 20 μm has been investigated across the full range of parameter values.

Within the ranges of parameter values given in table 1, there is no change in the general behaviour of the bubble – there is always an initial dissolution followed by bubble growth. However, the radius to which the bubble grows at $\tau = 600$ varies significantly in comparison to the 'base case' – the case in which all parameter values are at the mid-point of their ranges. When altering only one parameter from its mid-point value, varying surface tension has the least effect; bubble size at $\tau = 600$ differs by less than 0.3 % from the base case despite a ± 10 % change in the parameter value, with lower surface tensions leading to slightly greater growth. Altering Henry's constant shows a variation of around 4 % within the quoted parameter range (± 7 % change in parameter value), with greater solubility giving increased bubble growth. The parameter with the greatest variation in parameter range, and the greatest effect on the bubble size, is the diffusion coefficient, with a variation in value from the base case of over ± 20 %. As would be expected, growth rate increases with increased diffusion coefficient.

Given that the values of Henry's constant, diffusion coefficient and surface tension are not constant, but are known to lie within a certain range, model-based predictions of the maximum and minimum possible bubble growth were sought to enable comparison with experimental results. Figure 5 shows the theoretical upper (thick dotted) and lower (thick dashed) bounds of the growth of a bubble in xanthan gum,

https://doi.org/10.1017/S0022112010003472 Published online by Cambridge University Press

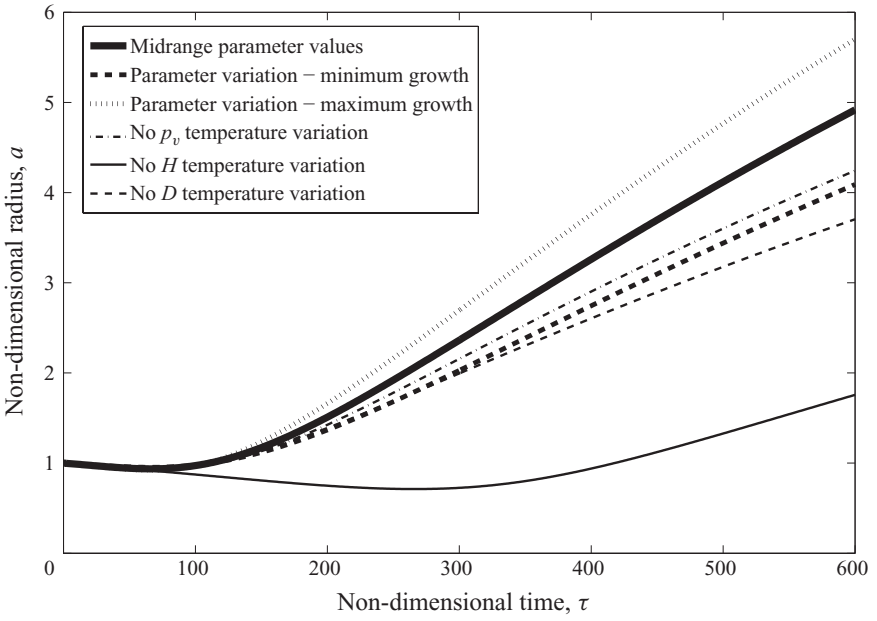


FIGURE 5. Effect of parameter variations on the behaviour of a 20 μm bubble in xanthan gum. The 'base case' for comparison is shown by the thick solid line; dotted and dot-dashed thicker lines show the bounds of bubble behaviour given the ranges of parameter values in table 1. The thinner lines give predictions of bubble behaviour omitting the temperature dependence of Henry's constant H (solid), vapour pressure p_v (dash-dotted) and diffusion coefficient D (dashed).

given the possible range of parameter values. The upper bound on growth is obtained using the maximum parameter values for Henry's constant and diffusion coefficient, and the minimum value for surface tension. Using the opposite extremes in parameter values yields the lower bound on bubble growth. The base case is shown as a thick black solid line for comparison.

The quantification of the effects above is for a 20 μm bubble. The role of surface tension will vary significantly with bubble size, as the Laplace pressure varies as $1/R$, making this a more important parameter at smaller bubble radii. The relative effects of Henry's constant and the diffusion coefficient are, however, relatively consistent with bubble radius. The exact values that the parameters take will be most important near to the radius threshold, where they are key in determining whether the bubble grows or dissolves.

4.3. *Importance of the inclusion of temperature dependence*

To understand the importance of including temperature-variant parameter properties in the model, each of the parameter temperature dependences was removed to ascertain changes in the bubble behaviour. Due to its key role in determining the concentration profile within the liquid, Henry's constant has the greatest effect on the behaviour of a bubble. If the temperature dependence is not present, the smallest bubbles may never grow, independent of the rate of heating.

The presence of the temperature dependences of diffusion coefficient, vapour pressure and surface tension are, respectively, of decreasing importance – the latter is so minimal that the bubble response is almost independent of the inclusion of the temperature dependence at initial radius $R_0 = 20\,\mu$m. The effect of the other three

https://doi.org/10.1017/S0022112010003472 Published online by Cambridge University Press

parameters is illustrated in figure 5 for a bubble above the threshold radius. The increase of vapour pressure and diffusion coefficient with time increases the rate of bubble growth, although these changes are not key in determining the general bubble behaviour. However, the time dynamics of the bubble response are significantly altered, should the temperature-dependent changes in Henry's constant be neglected, although in this case the bubble does still grow. The bubble growth predicted is still a diffusion-driven process, but instead of the concentration gradient switching in direction due to a reduction in overall solubility and liquid supersaturation, the gradient switches due to increasing vapour pressure within the bubble reducing the internal gas pressure below the ambient value. Although the effect of removing temperature dependences of vapour pressure and Henry's constant is the same irrespective of the bubble size, in that the bubble size is reduced at any point in time, the radius threshold is important when considering the effect of the temperature dependence of the diffusion coefficient. Removing the temperature dependence of the diffusion coefficient slows the diffusion process, independent of its direction; hence bubbles below the radius threshold dissolve more slowly and those above it grow more slowly than when the temperature dependence is present.

From this analysis, it can be seen that the inclusion of the temperature dependences of vapour pressure, Henry's constant and diffusion coefficient are important in predicting the response of a bubble to an arbitrary temperature profile, whereas the temperature dependence of surface tension can safely be neglected without any distinguishable change to the model predictions.

5. Experimental set-up and procedure

A 0.5 % xanthan gum solution was prepared by dissolving 0.4 g of food-grade xanthan gum powder in 80 ml of filtered deionised water. As hydrated xanthan has the tendency to aggregate into clumps, the powder was added slowly to the water, with a magnetic stirrer employed to ensure thorough mixing. It is during this mixing process that small air bubbles become trapped within the gel matrix formed by the hydrated xanthan polymer chains. The viscosity of xanthan gum is sufficient to counter the effects of buoyancy, and hence stop the bubbles rising quickly to the surface of the gel.

The experimental set-up is shown in figure 6. A symmetrical design using two identical 100 Ω resistors (Multicomp MC14659) was chosen to minimize thermal convection within the gel, and hence reduce the translation of the bubbles within it. Evaporation of the gel during experiments was also a concern, and this was minimized by the addition of a Perspex lid to the phantom holder. A series of 1 mm diameter holes were added at 5 mm intervals for the positioning of thermocouples used to monitor the temperature field within the gel. Power was provided by a DC power supply (HP Agilent E3630A) allowing heating inputs of 0–4 W per resistor.

Photographs of the bubbles in the gel phantom were taken using a 10.1 megapixel digital SLR Camera (Canon EOS 400D, 3888×2592 pixels) with a 5× macro lens (Canon MP-E 65); the area of focus was approximately $4\,\text{mm} \times 3\,\text{mm}$ giving a resolution of approximately $1.15\,\mu\text{m pixel}^{-1}$. The camera was connected to a PC via a Universal Serial Bus (USB) interface, and remotely controlled using the bundled Canon EOS Utility, allowing photographs to be taken at fixed time intervals of 30 s throughout the duration of the experiment. The best picture quality was obtained using a small aperture (f13) and a 1.6 s exposure time at speed ISO100 in full manual mode. The small aperture was chosen to maximize depth of field, approximately 0.25 mm

https://doi.org/10.1017/S0022112010003472 Published online by Cambridge University Press

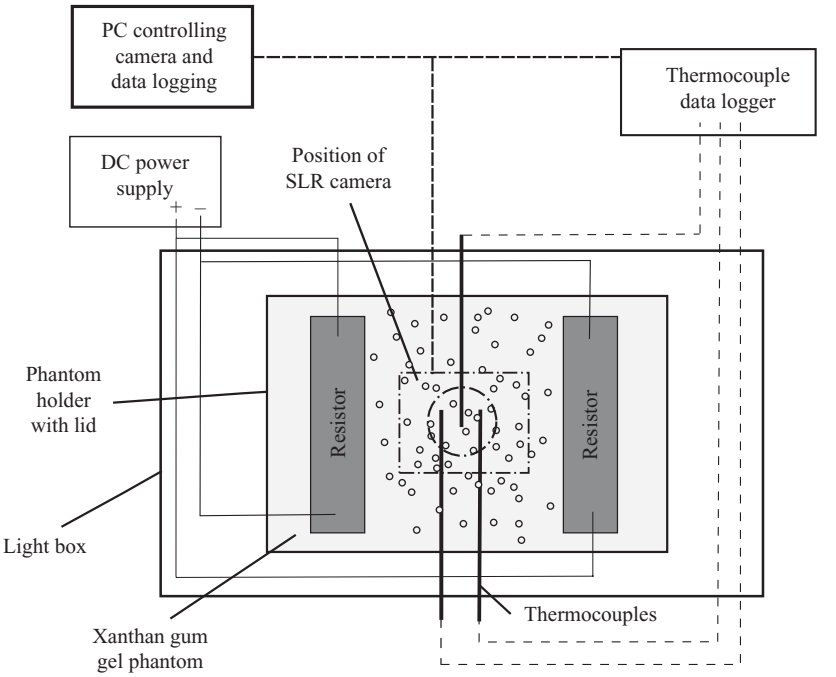


FIGURE 6. Diagram of experimental set-up.

at these settings, and ensure the bubbles photographed were in focus throughout the entire duration of the experiment. However, this results in diffraction-limited images and accordingly there will be some diffraction broadening of the bubbles, which will be of greater importance at smaller bubble radii. A fluorescent backlight (Jessops Lightbox 6 in. × 9 in.) was used to maximize contrast between the bubbles and surrounding medium and reduce any shadowing from other light sources, whilst minimizing any additional heating effect.

Temperatures were measured using three T-type thermocouples (Omega Engineering HYP-2 with SMP connector) at variable locations in the phantom holder, with a 5 mm spacing between thermocouples. The temperature data were recorded on a PC via a USB-linked data logger (Picotech TC-08) using the bundled Picotech software (Picolog recorder) simultaneously with data acquisition from the camera. The temperature profiles recorded were subsequently used in the theoretical model to predict the radius–time profiles of specific bubbles. The camera was positioned centrally between the two resistors, such that either one thermocouple was visible in centre frame, or the field of view was between two adjacent thermocouples. As a result of the symmetrical nature of the spatial temperature field, there was little spatial variation ($<1\,^{\circ}$C) of the temperature profile across the field of view in this area at all times, and hence all bubbles were assumed to experience the same temperature variation.

6. Image analysis

To allow comparison with model predictions, an algorithm based on an edge-detection method has been developed to compute bubble radii across the experimentally obtained photograph sequences. As translation of bubbles is likely,

https://doi.org/10.1017/S0022112010003472 Published online by Cambridge University Press

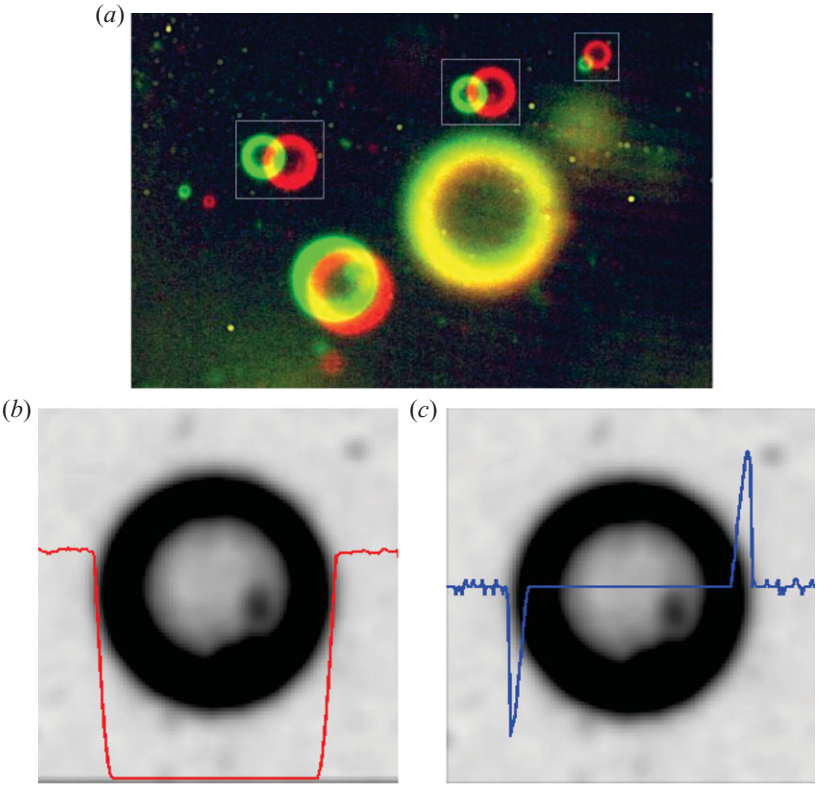


FIGURE 7. (*a*) Superposition of photographs from the beginning (red) and end (green) of the experimental sequence; white bounding boxes indicate 'regions of interest' tracked through the sequence of photographs. (*b*, *c*) Edge detection for sizing bubbles; the superposed lines show the minimum pixel value (red) and its associated gradient (blue).

due to convection, it is necessary to account for any frame-to-frame movement to enable tracking of bubbles across the full sequence. The translation is visualized by superposing the images from the start and end of the sequence in separate primary channels – the first image forms the red channel, with the final image forming the green channel – resulting in an image such as that of figure 7(*a*). Superposition of the images also allows the immediate visualization of the nature of size changes in the bubble population during the course of the experiment.

The edge-detection algorithm developed is most accurate when there is a single in-focus bubble within the frame. A set of regions of interest is manually selected from the overlaid photographs, with each region containing a single bubble; these regions are identified by a surrounding white rectangular box, as illustrated in figure 7(*a*). To find the edges of the bubble, the minimum pixel value for each row and each column is found, and two orthogonal curves of such minima are constructed, one of which is shown in figure 7(*b*). As the minimum pixel value changes most rapidly across the bubble wall, the position of the maximum gradients will correspond to these points (figure 7*c*). The bubble radius is then computed as the mean of the bubble radii as found in the two orthogonal directions; should these values differ by more than 10 % the output from the automatic algorithm is flagged and a manual sizing method used to confirm the radius value. The manual sizing method involves the selection on

https://doi.org/10.1017/S0022112010003472 Published online by Cambridge University Press

screen of the top, bottom, leftmost and rightmost points on the bubble boundary; the bubble radius is then found from an average of the two radii, as with the automatic method. A comparison between the automatic and manual methods showed the two to be near-equivalent, with a mean error of less than one pixel.

By following each of the defined regions throughout the sequence of photographs, the evolution of the bubble radius over time is tracked. The radius–time curves produced can then be compared against those predicted by the numerical solver using the corresponding thermocouple data.

7. Model comparison

7.1. *Bubble dissolution with no external heating*

To verify the experimental technique and to confirm that the values of xanthan gum parameters obtained from the literature were correct, an initial set of experiments without any external heat input were conducted. As was expected, all of the bubbles were found to dissolve.

Without any external heating, the model developed is greatly simplified, as temperature dependences do not have to be taken into account. In the case of bubble dissolution in xanthan gum, the time scales are such that a quasi-steady-state gas concentration profile can be assumed, and an analytical solution for the bubble-dissolution time obtained. As all bubbles of the same radius contain the same mass of gas, dissolution time must be solely dependent on bubble radius for a bubble in a particular medium. It can further be shown that the rate of change of mass is only dependent on the physical parameters of the medium, and hence all bubbles will dissolve along the same radius–time profile. Therefore, the rate of dissolution is the same for all bubbles of a particular radius, giving a simple comparative measure. The relationship between bubble size and rate of dissolution can be expressed as:

$$\dot{R} = \frac{-6R_g T \sigma H D}{3R^2 p_\infty + 4\sigma R}. \tag{7.1}$$

Although the resolution of the optical set-up is good, a quantization error will be present, and very slight changes in position of the bubble and picture clarity will result in errors in sizing. To compensate for these inaccuracies, a five-point moving average is calculated for the experimentally obtained radii and assigned to the central (third) member of each five-point set. As the average calculated will still not be an exact measure of the bubble size, the bubble radii are grouped into 2 μm wide 'bins'; this allows a measure of variation in the observed rates of collapse at a particular bubble 'size' to be computed. The dissolution rate associated with the centre point of the five-point set is then calculated using the gradient of the line of best fit through these five points. Plotting the set of dissolution rates for a particular radius bin and finding the standard deviation of the computed rates of collapse for 32 bubbles across four experiments results in figure 8. The predicted region for xanthan gum, based on the range of parameter values in table 1, lies between the solid black curves, and the predicted curve for bubbles in water is shown as the black dotted line.

The experimental results show good agreement with the analytically predicted region, and hence agree with the values measured by Teresaka & Shibata (2003). The theoretical curve for water lies some distance below the majority of the experimental measurements, which shows the importance of using the correct set of parameter values for the medium in question. The bubble-wall velocities recorded in figure 8 can also be used to justify the assumption that allows the inertial terms in the

https://doi.org/10.1017/S0022112010003472 Published online by Cambridge University Press

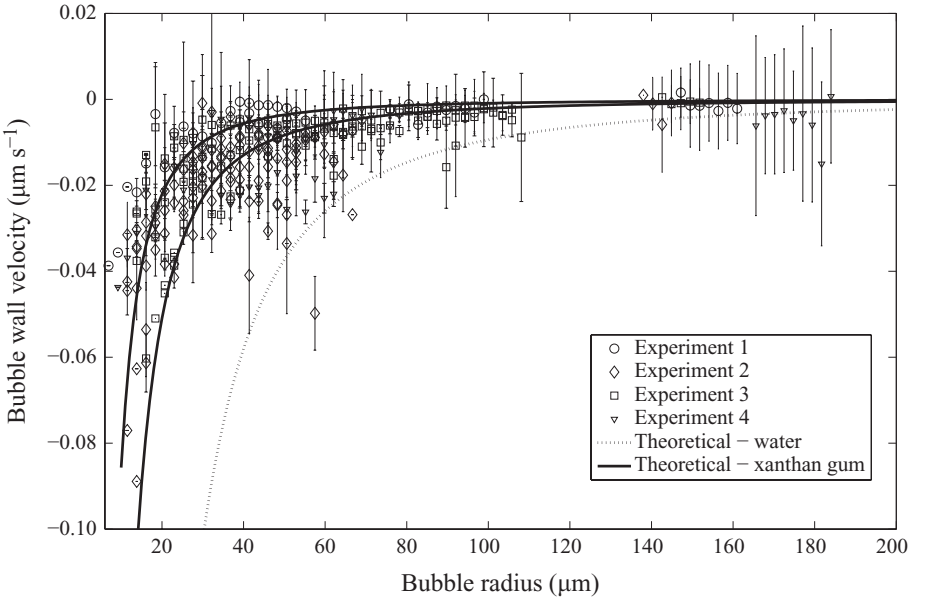


FIGURE 8. Comparison of experimental data for bubble-dissolution rates (thin vertical lines) with analytical predictions, for xanthan gum (region between solid lines) and water (dotted line).

Rayleigh–Plesset equation to be neglected. Micrometre-sized bubbles have collapse velocities of the order of tens of micrometres per second, a value which decreases as bubble size increases, meaning the inertial terms will take values several orders of magnitude below the smallest pressure term. The viscous stress term $4\eta\dot{R}/R$, even for a viscosity as high as 1 Pa s, has a magnitude of less than 1 Pa for bubbles greater than 7 μm and only becomes comparable to the vapour pressure term for bubbles of sub-micrometre sizes. The use of an 'equilibrium' pressure balance, rather than the full Rayleigh–Plesset equation, is therefore acceptable for diffusion-controlled processes on these time scales.

7.2. *Bubble response to heating*

By varying the input voltage across the pair of resistors in the experimental set-up, a wide variety of heating rates and profiles were used to heat the bubbly xanthan gum medium. The range of temperature profiles cannot easily be described by a single parameter, so comparison between experimental observations and the theoretical model is achieved by inputting the exact temperature profile, as measured by the thermocouples, and the initial bubble radii into the numerical solver. This allows the radius–time response specific to a particular bubble and heating profile to be obtained.

The measured temperature profiles from three different experiments, covering a wide range of heating rates, are shown in figure 9(*a*). Using the temperature curve labelled (a), the upper and lower bounds of the predicted responses of a 47 μm bubble from this experiment are calculated and shown in figure 9(*b*). It is immediately clear that the model is not capturing the general behaviour of the bubble's response to the heating, predicting a continuing rise in the bubble growth, which is in contrast to the slowing of the bubble growth shown in the experimental results. The experimental radius–time profiles therefore suggest that a factor limits the bubble growth after a

https://doi.org/10.1017/S0022112010003472 Published online by Cambridge University Press

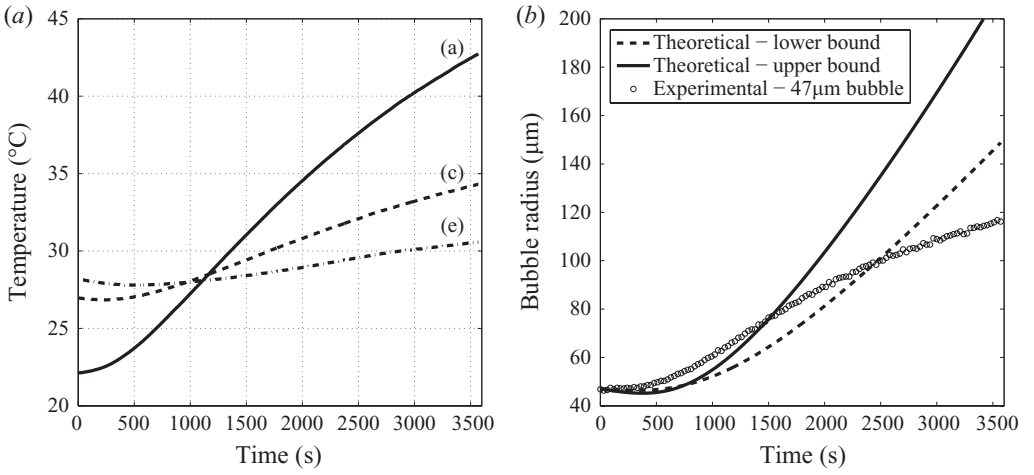


FIGURE 9. (*a*) Temperature profiles obtained from thermocouple measurements in three separate experiments. (*b*) Comparison of experimental observations and predicted region of response (bounded by solid/dashed lines) of a 47 μm bubble in xanthan gum, in response to heating profile (a).

certain time; it is postulated that, due to the bulk liquid containing many bubbles in close proximity, the supply of gas for continued growth may be limited or even exhausted by the rapidly expanding bubble. Although the model presented considers gas diffusion only to be occurring in a thin region surrounding the bubble, the fixed-value BC on the outer edge of the diffusion layer still theoretically allows gas to diffuse into and out of the remainder of the bulk liquid to maintain this concentration value and hence allow 'infinite' growth.

The model is therefore altered at this point to limit the supply of gas available to the bubble; this is achieved by altering the BC on the outer edge of the diffusion layer from one of fixed value to one of zero gradient, as used by Arefmanesh *et al.* (1992). This ensures that gas can no longer diffuse into or out of the diffusion layer. Implementation in the numerical solver is through use of a second-order Taylor expansion for the gradient at the outer edge, resulting in the condition:

$$3c'_k + c'_{k-2} - 4c'_{k-1} = 0, \tag{7.2}$$

where k is the number of spatial grid points. The result is a small change in the Crank–Nicolson matrix used in the solution of the diffusion equation. In the subsequent theoretical predictions, the diffusion layer surrounding the bubble was limited to a constant width of 0.5 mm. Although the proximity of one bubble to another varied considerably, this value was chosen based on the presence of approximately 20–25 bubbles in each 4 mm × 3 mm field of view.

Using the revised model, the behaviour of bubbles of a range of sizes was predicted for all temperature profiles of figure 9(*a*), and plotted alongside the measured radius–time profiles from the experiments. Temperature-dependent properties, and hence saturation concentration within the bulk liquid, were at first calculated for the initial experimentally recorded temperature. As figure 10(*a*, *c*, *e*) shows, the revised model no longer predicts a near-constant bubble growth-rate with time; the growth of larger bubbles does continue but the growth-rate slows significantly after an initial faster expansion. The general behaviour of the larger bubbles is now captured well by the model predictions. However, for bubbles of smaller initial radius, the experimental

https://doi.org/10.1017/S0022112010003472 Published online by Cambridge University Press

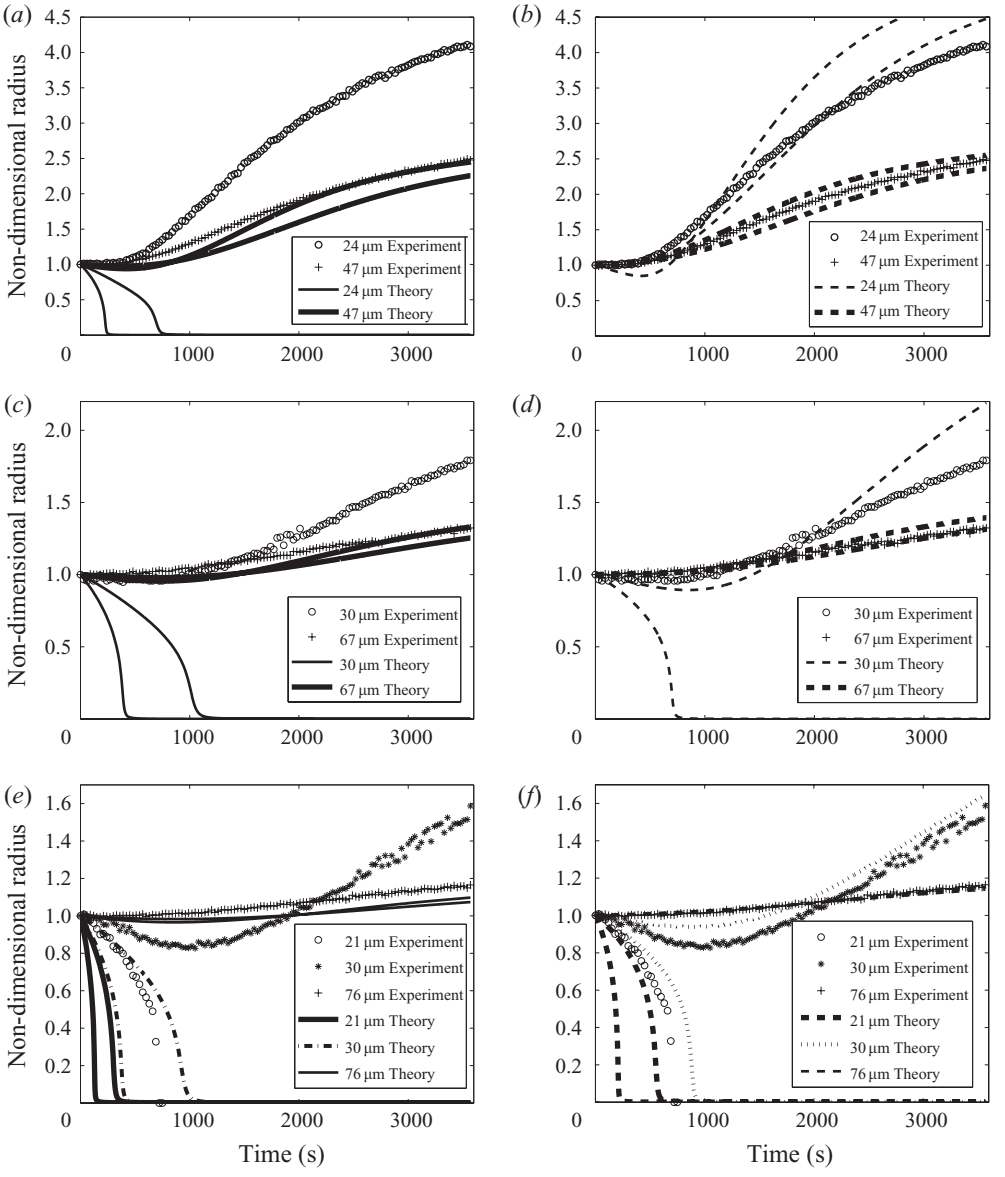


FIGURE 10. Comparison of experimental observations (Experiment) and predicted responses (Theory) of bubbles with limited gas availability in xanthan gum at various heating rates; the bubble responses in each of the left-hand plots are due to the correspondingly lettered temperature profile of figure 9(*a*). (*a*, *c*, *e*) The predicted bubble responses using saturation concentration calculated from initial temperature; (*b*, *d*, *f*) the corresponding plots using slightly raised (2–4 %) saturation concentrations. The theoretical predictions are given as upper and lower bounds of bubble behaviour, using the extremes of the xanthan parameter ranges as discussed in § 4.2; it is expected the bubble behaviour should lie between these bounds.

observations often show bubble growth whereas the model predicts dissolution – in general the behaviour of the bubble response is not predicted well by the model for these bubble sizes, even when considering the wide range of values that the xanthan gum parameters can take.

https://doi.org/10.1017/S0022112010003472 Published online by Cambridge University Press

A closer comparison of the bubble responses shows that model and experiment do not correspond well early on in most of the traces – the model predicts that bubble growth will begin later than is observed experimentally, and that bubble dissolution will occur more rapidly than is seen in experiments. Smaller bubbles that can be seen in the experiments to grow, or to dissolve and then grow, are all predicted by the model to dissolve away entirely. These discrepancies suggest that the difference in concentrations between the bulk liquid and at the bubble wall could in reality be lower than the calculated value in the model.

A small increase in the dissolved gas concentration would be expected from the dissolution of bubbles within the liquid prior to the start of heating. The bubble population is likely to include many micron and sub-micrometre sized bubbles that are invisible to the optical set-up used, and hence the exact increase in gas concentration is difficult to quantify. Figure 10(b, d, f) shows that an increase in the saturation concentration of the order of 2–4 % (equivalent to a 1–2K change in temperature) can significantly alter the predictions of the model for a specific temperature input. Although still not a perfect match, the basic time-dynamics of every bubble, whether it grows, dissolves or dissolves then grows, are now predicted to a good degree of accuracy in the majority of cases. This demonstrates that the value of the gas concentration in the bulk liquid is key in determining the nature of the bubble response caused by an arbitrary heating profile.

As heating continues, thermal equilibrium will be attained and, over time, a new saturation concentration will be reached. As the solution is now at a higher temperature, this concentration will be of a lower value than that at the beginning of the heating. Bubbles that are growing due to heating are slowly exhausting the supply of dissolved gas within the liquid, as shown in figure 10 by the decreasing growth rate with time. In the long term, the lack of gas for diffusion in the surrounding liquid, or the lower value of the gas saturation concentration at the elevated temperature, will reassert the concentration gradient present pre-heating and gas will diffuse out of the bubble. Therefore, even though a bubble can grow if it is heated quickly enough, it will eventually dissolve away as conditions re-equilibrate at the higher temperature.

8. Discussion

The comparisons of figure 10 show that predicting the exact response of a bubble to an arbitrary time-variant temperature profile is difficult to achieve. The main difficulties arise due to limited knowledge of the form of, and parameter values describing, the gas concentration profile within the bulk liquid; such values will vary significantly between different media and among bubbles within a single-bubble population. However, it is clear that inclusion of the relevant temperature dependences, especially that of Henry's constant, are key in obtaining accurate predictions of bubble behaviour. The close agreement of the bubble dynamics seen in experiments and predicted by the model shows that the bubble growth and dissolution is a diffusion-driven process, rather than one solely due to thermal expansion and increased vapour pressure.

The diffraction-limited nature of the optical set-up will mean that the measurements of the bubble radii will be slightly larger than the actual sizes. The exact difference in size is difficult to ascertain due to unknowns about the camera optics and the robustness of the sizing algorithm to the varying image contrasts that occur at different bubble sizes, and to the softening of the bubble edge caused by diffraction broadening. However, an experimental calibration suggests that the maximum error is of the order of 3 μm. With the actual bubble size being smaller than measured, a

https://doi.org/10.1017/S0022112010003472 Published online by Cambridge University Press

smaller radius should be used in the numerical solver for a more accurate comparison, but this will result in a greater mismatch than is currently predicted. Diffraction, therefore, cannot account for the difference seen between theory and experiment in figure 10.

It has been demonstrated that the temporal dynamics of bubble growth and dissolution are very sensitive to small changes in the gas distribution surrounding a bubble. Of the assumptions made in the construction of the model, those of the value of the saturation concentration, the initial concentration profile and the width of the diffusion layer will all have an effect on how the nature of the concentration profile varies with time, and hence the exact form of the bubble response. Additionally, the parameter temperature dependences have been based on those in water rather than in xanthan gum, and although the xanthan gum phantom is composed of over 99 % water, the difference in the key parameter values shows that the polymeric nature of the xanthan chains does result in differences in the behaviour of the two substances.

Figure 10 shows that small changes in saturation concentration levels can result in significant changes in predicted bubble behaviour. These changes are greater than may be expected because the difference between the gas concentration at the bubble wall and the saturation concentration, rather than the saturation concentration itself, is the significant value that determines the bubble behaviour. Small percentage changes in saturation concentration will result in significant lowering of the concentration difference between the bubble wall and the bulk liquid, which for larger bubbles can cause a complete reversal of the concentration gradient at the bubble wall and immediate growth. For smaller bubbles, lower concentration differences will reduce the radius-threshold necessary for a bubble to grow, and slow the dissolution of smaller bubbles for a particular heating profile. The change occurs as a smaller increase in temperature is now sufficient to cause the necessary reduction in Henry's constant that results in bubble growth. An accurate experimental determination of the bulk-liquid saturation concentration would reveal whether values are higher than calculated from the measured temperature, and hence whether the postulation made in § 7.2 is correct.

Changing the value of bulk-liquid saturation concentration has a more pronounced effect on the behaviour of bubbles of smaller initial radii, as shown by the differences between figures 10(a,c,e) and 10(b,d,f). To explain this variation in behaviour, the relative ratio of transferred mass to bubble mass needs to be considered. Whereas the amount of mass within the bubble is proportional to radius cubed, transferred mass can be shown to be approximately proportional to the bubble radius. Bubbles of larger radii have high initial mass, and so the amount of gas diffusing into or out of a larger bubble is small relative to that already within its walls. The bubble is therefore more robust to small changes in the local environment – inevitably growing in response to an increase in temperature. In contrast, the amount of gas diffusing through the bubble wall for smaller bubbles is more significant than that for larger bubbles, when compared with the initial bubble mass. A small change in saturation concentration, especially for those bubbles close to the radius-threshold of a particular temperature profile, can result in a complete change in bubble behaviour – growth where there was once dissolution, or vice versa.

Given the sensitivity of the bubble response to the relative difference between bubble wall and saturation gas concentrations, it follows that the exact nature of the initial gas concentration profile around a bubble will also have an effect on the subsequent time-dynamics of the bubble response. The assumed equilibrium profile will be more appropriate than a step-change based profile, as the bubbles have existed in the medium for some time before heating commences. However, as noted when

https://doi.org/10.1017/S0022112010003472 Published online by Cambridge University Press

considering the set-up of the numerical solver, the exact value of the concentration gradient at the bubble wall is a key factor in determining subsequent bubble behaviour. A more accurate determination of the value of the concentration gradient, calculated from a better-known concentration profile, would therefore result in a more realistic radius–time profile.

It is fairly intuitive to see that restriction or expansion of the diffusion layer, relative to the arbitrary 0.5 mm limit chosen, will change the quantity of gas available for diffusion. The exact size that a bubble can grow to, or the rate at which a bubble dissolves, will differ dependent on this value. In the experiments carried out, there was no control over the distribution of bubbles and bubble sizes within the xanthan gum. This led to some bubbles being in close proximity to others, whilst in other regions there could be separations of several bubble radii. The actual amount of gas available for growth of any particular bubble is therefore highly variable. Further investigation using the model suggests that the best matches between theory and experiment occur when using a diffusion layer width of approximately 8–12 times that of the bubble radius. The assumption of a one-dimensional system also comes into question when considering the gas concentration distribution around the bubble – 'competition' for gas between growing bubbles, extra dissolved gas within the bulk liquid that has diffused out of a dissolving bubble, and large expanses of liquid with no bubbles present will all break the spherical symmetry that the model assumes.

Although it is not an issue in this study, due to the limited resolution of the optical set-up, the accuracy of calculations for very small bubbles could be called into question owing to the short time periods over which changes in the bubble radius are occurring. The assumption that the temporal dynamics are slow enough to neglect the inertial terms in the Rayleigh–Plesset equation may no longer be valid when considering small bubble radii with dissolution times of the order of seconds, rather than minutes.

The model in its current state is open to several modifications to increase its suitability in describing real-world applications. Introduction of parameters to account for dissolution or growth in viscoelastic liquids, in addition to simple liquids like water, will allow the bubble response in a much greater range of materials and media to be modelled. In processes such as the rising of dough caused by yeast, the generation of additional gas(es) through chemical or biological processes would be necessary to accurately describe the evolution of bubbles. Finally, the model would need significant adaptation should there be an external driving force acting on the bubbles, so as to fully describe the inertial and diffusion characteristics of a multi-time-scale problem and account for phenomena such as rectified diffusion during acoustic cavitation.

In many of the situations arising, where application of such a model would be of use, it is accepted that the accurate determination of many of the parameter values and properties discussed above will be very difficult to achieve. However, often it will not be necessary to know the exact radius–time profile of a bubble's evolution; knowledge of the basic temperature-dependent parameters, and the expected void fraction and bubble size distribution would be sufficient to obtain a general overview of the dynamics of a bubble population from the model.

9. Conclusions

A single-bubble model in liquid has been developed to describe the dynamics of bubbles undergoing an arbitrary time-variant change in temperature. For a particular heating profile, the model predicts a range of bubble behaviours and a threshold for

https://doi.org/10.1017/S0022112010003472 Published online by Cambridge University Press

bubble growth that are both dependent on the initial bubble radius. An investigation into the effect of each of the temperature dependences on the model predictions has shown it essential to include the temperature dependence of Henry's constant to allow accurate prediction of the time-dynamics of bubble growth or dissolution; the dependences of diffusion coefficient and vapour pressure are of decreasingly lower importance, whereas that of surface tension can be neglected without any detectable change to the predictions.

Experimental validation in xanthan gum gel phantoms has shown that using the correct parameter values for xanthan gum is key in obtaining agreement with model predictions for bubbles dissolving without any external heating. When a bubbly mixture is heated, agreement between model and experiment is only seen when the amount of dissolved gas available for bubble growth within the theoretical model is limited. The effect of small changes in the value of the gas saturation concentration, especially on the response of smaller-radii bubbles and those close to the radius-threshold, is shown to be significant in the ability to accurately predict the radius–time evolution of a bubble in a time-variant temperature field.

REFERENCES

Arefmanesh, A., Advani, S. G. & Michaelides, E. E. 1992 An accurate numerical solution for mass diffusion-induced bubble growth in viscous liquids containing limited dissolved gas. *Intl J. Heat Mass Transfer* **35**, 1711–1722.

Barlow, E. J. & Langlois, W. E. 1962 Diffusion of gas from a liquid into an expanding bubble. *IBM J.* **6**, 329–337.

Cable, M. & Frade, J. R. 1987 Diffusion-controlled growth of multi-component gas bubbles. *J. Mater. Sci.* **22**, 919–924.

Church, C. C. 2005 Frequency, pulse length, and the mechanical index. *Acoust. Res. Lett. Online* **6**, 162–168.

Coussios, C. C. & Roy, R. A. 2008 Applications of acoustics and cavitation to noninvasive therapy and drug delivery. *Annu. Rev. Fluid Mech.* **40**, 395–420.

Divinis, N., Kostoglou, M., Karapantsios, T. D. & Bontozoglou, V. 2005 Self-similar growth of a gas bubble induced by localized heating: the effect of temperature-dependent transport properties. *Chem. Engng Sci.* **60**, 1673–1683.

Epstein, P. S. & Plesset, M. S. 1950 On the stability of gas bubbles in liquid–gas solutions. *J. Chem. Phys.* **18**, 1505–1509.

Fan, J., Mitchell, J. R. & Blanshard, J. M. V. 1999 A model for the oven rise of dough during baking. *J. Food Engng* **41**, 69–77.

Filimonov, V. E. 1991 Equations for the computer calculation of the partial water vapor pressure and of the dew point of humid air. *Chem. Pet. Engng* **27**, 254–256.

Fyrillas, M. M. & Szeri, A. J. 1994 Dissolution or growth of soluble spherical oscillating bubbles. *J. Fluid Mech.* **277**, 381–407.

Han, P. & Bartels, D. M. 1996 Temperature dependence of oxygen diffusion in H_2O and D_2O. *J. Phys. Chem.* **100**, 5597–5602.

IAPWS 1994 *IAPWS Release on Surface Tension of Ordinary Water Substance*. Available at http://www.iapws.org/

Miyatake, O., Tanaka, I. & Lior, N. 1994 Bubble growth in superheated solutions with a non-volatile solute. *Chem. Engng Sci.* **49**, 1301–1312.

Rabkin, B. A., Zderic, V. & Vaezy, S. 2005 Hyperecho in ultrasound images of HIFU therapy: involvement of cavitation. *Ultrasound Med. Biol.* **31**, 947–956.

Rayleigh, L. 1917 On the pressure developed in a liquid during the collapse of a spherical cavity. *Phil. Mag.* **34**, 94–98.

Rettich, T. R., Battino, R. & Wilhelm, E. 2000 Solubility of gases in liquids. 22. High-precision determination of Henry's law constants of oxygen in liquid water from $T = 274$ K to $T = 328$ K. *J. Chem. Thermodyn.* **32**, 1145–1156.

https://doi.org/10.1017/S0022112010003472 Published online by Cambridge University Press

Riemer, B., Haines, J., Wendel, M., Bauer, G., Futakawa, M., Hasegawa, S. & Kogawa, H. 2005 Cavitation damage experiments for mercury spallation targets at the LANSCE-WNR in 2005. *J. Nucl. Mater.* **377**, 162–173.

Robinson, A. J. & Judd, R. L. 2001 Bubble growth in a uniform and spatially distributed temperature field. *Intl J. Heat Mass Transfer* **44**, 2699–2710.

Schafer, R., Merten, C. & Eigenberger, G. 2002 Bubble size distributions in a bubble column reactor under industrial conditions. *Exp. Therm. Fluid Sci.* **26**, 595–604.

Scriven, L. E. 1959 On the dynamics of phase growth. *Chem. Engng Sci.* **10**, 1–13.

Teresaka, K. & Shibata, H. 2003 Oxygen transfer in viscous non-Newtonian liquids having yield stress in bubble columns. *Chem. Engng Sci* **58**, 5331–5337.

Zahringer, K., Martin, J.-P. & Petit, J.-P. 2001 Numerical simulation of bubble growth in expanding perlite. *J. Mater. Sci.* **36**, 2691–2705.

https://doi.org/10.1017/S0022112010003472 Published online by Cambridge University Press